

# Supplementary Material for Holographic Glasses for Virtual Reality

JONGHYUN KIM, NVIDIA and Stanford University

MANU GOPAKUMAR, SUYEON CHOI, AND YIFAN PENG, Stanford University

WARD LOPES, NVIDIA

GORDON WETZSTEIN, Stanford University

## ACM Reference Format:

Jonghyun Kim, Manu Gopakumar, Suyeon Choi, and Yifan Peng, Ward Lopes, and Gordon Wetzstein. 2022. Supplementary Material for Holographic Glasses for Virtual Reality. 1, 1 (August 2022), 9 pages. <https://doi.org/10.1145/3528233.3530739>

## A IMPLEMENTATION DETAILS

### A.1 Hardware Implementation

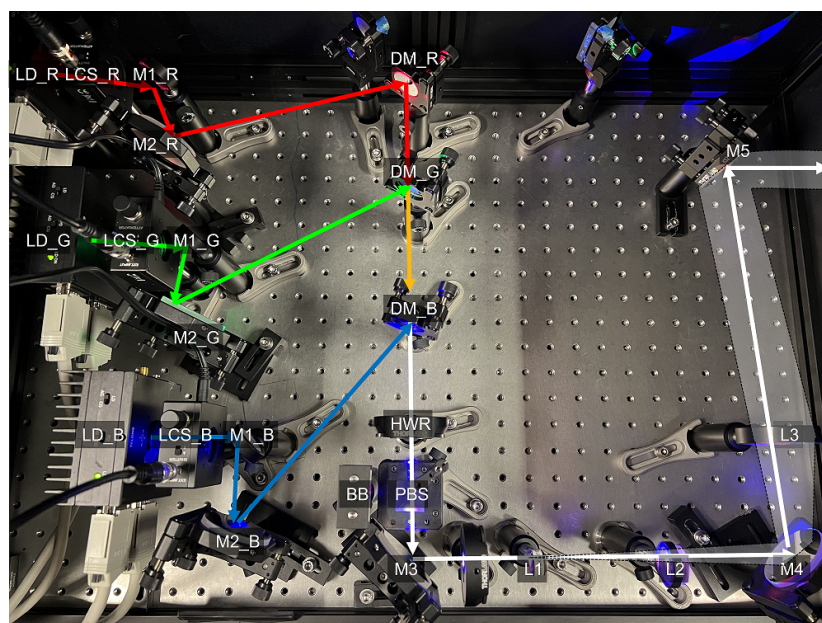


Fig. S1. Photo of the implemented synchronized color sequential coherent light source. LD is laser diode, LCS is liquid crystal shutter, M1,M2,M3,M4,M5 are planar mirrors, DM is dichroic mirror, HWR is a half wave retarder, BB is a beam block, L1, L2, L3 are achromat lenses, and PBS is a polarized beam splitter. Note that the collimated coherent light source is coming out from the small hole on the right wall.

**A.1.1 Synchronized color sequential coherent light source.** Figure S1 shows the implemented synchronized color sequential coherent light source. each color laser diode (R,G,B) mounted on a temperature-controlled mount (Thorlabs LDM56/M) were controlled by a temperature controller (Thorlabs TED200C) and a laser diode driver (Thorlabs LDC220C), respectively. These coherent light sources were sequentially controlled by 3 liquid crystal shutters (Thorlabs LCC1620/M), which were controlled by the external trigger that was generated from the SLM (Holoeye LETO-3). 3-color beams were combined through dichroic mirrors, then expanded and collimated with achromat lenses (L1, L2, L3). The individual intensity was controlled by the laser diode driver, while the overall intensity was controlled by a polarized beam splitter

---

Authors' addresses: Jonghyun Kim, NVIDIA , Stanford University, [jonghyunk@nvidia.com](mailto:jonghyunk@nvidia.com); Manu Gopakumar, Suyeon Choi, and Yifan Peng, Stanford University; Ward Lopes, NVIDIA; Gordon Wetzstein, Stanford University, [gordonwz@stanford.edu](mailto:gordonwz@stanford.edu).

Permission to make digital or hard copies of all or part of this work for personal or classroom use is granted without fee provided that copies are not made or distributed for profit or commercial advantage and that copies bear this notice and the full citation on the first page. Copyrights for components of this work owned by others than ACM must be honored. Abstracting with credit is permitted. To copy otherwise, or republish, to post on servers or to redistribute to lists, requires prior specific permission and/or a fee. Request permissions from [permissions@acm.org](mailto:permissions@acm.org).

© 2022 Association for Computing Machinery.

XXXX-XXXX/2022/8-ART \$15.00

<https://doi.org/10.1145/3528233.3530739>

and a rotating half-wave retarder. The collimated light is coming out from the small hole on the right wall for the laser safety. Note that the miniaturized version of this system is commercially available (e.g. FISBA RGBeam) but we can precisely control the temperature, intensity, and the wavelength of the light source with the implemented system.

**A.1.2 GP lens details.** Figure S2 shows the characteristics of the geometric phase (GP) lens. The experimental setup was done with the benchtop prototype with and without the quarter-wave plate (QWP). Without QWP, the both right-handed circular polarization (RHCP) and left-handed circular polarization (LHCP) were refracted by the GP lens, and created both diverging and converging lights. With a QWP, the diverging light is successfully filtered out. However, due to the imperfect GP lens fill factor, an unwanted collimated light, which hasn't been modified with the GP lens, created a SLM-sized rectangle at the pupil plane as shown in the right of Fig. S2. This loss creates a bright region in the perceived image as shown in the captured results. However, since it is unmodified at all, it can be reduced with an additional right handed circular polarizer in front of the GP lens.

Figure S2 also shows the high-diffractive orders (HDOs) create repeated viewpoints at the pupil plane. Although these repeated HDOs are caused by the SLM structure, it systematically looks similar to the eye box expander scheme with a pupil replicating waveguide. Interestingly, each HDO shows the same holographic images too. One can propose an pupil replicating Holographic Glasses design by having a larger pixel pitch  $p_s$  and a longer focal length  $f_L$  to match the eye box  $w_e$  and  $w_h$ . By doing so, we can achieve continuous eye box. However, we do not recommend this because the intensity of HDOs are very low compared to the center lobe and the resolution gets lower due to the larger pixel pitch.

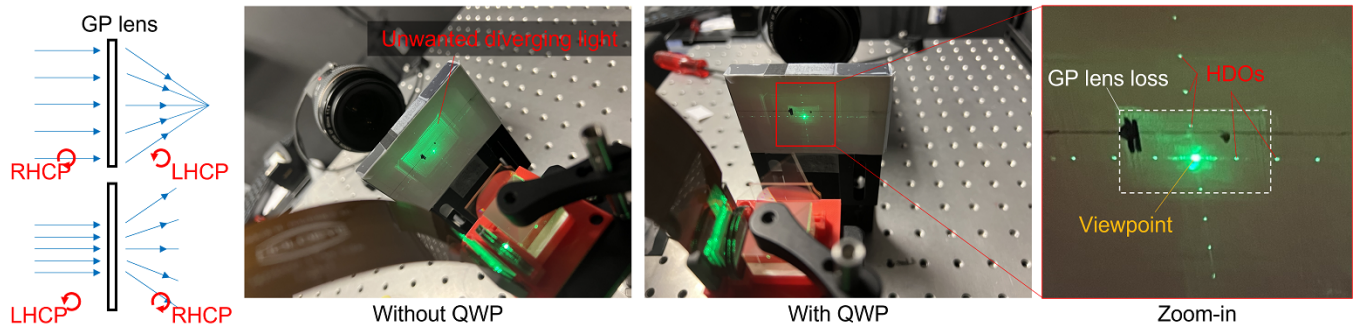


Fig. S2. Experimental results of the GP lens test. (left) Principle of the GP lens (center-left) Without QWP, the unwanted diverging light wasn't filtered out. (center-right) With QWP, the unwanted diverging light was filtered out. (right) The center viewpoint and the repeated HDOs were observed in the close-up photo. the white region is the loss from the GP lens.

**A.1.3 Virtual-mode holographic display.** In the previous research literature, holographic near-eye displays usually form holographic images in front of the SLM as shown in the left of Fig. S3. The holographic image, however, can be located behind the SLM as shown in the right of Fig. S3. In this paper, we applied virtual-mode holographic display for a smaller form factor and a bigger FOV.

See section 3.1.1 for more detailed information.

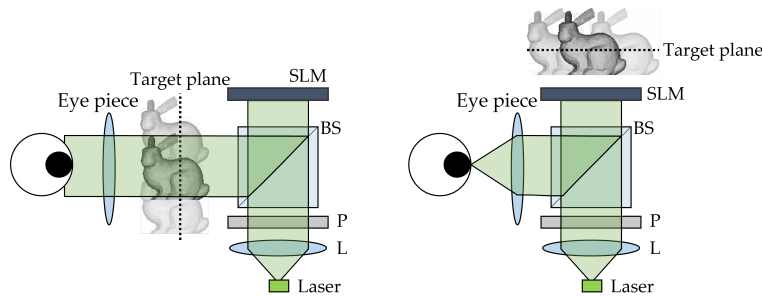


Fig. S3. Schematic diagram of (left) real-mode and (right) virtual-mode holographic near-eye display.  $L$  is a collimating lens,  $P$  is a linear polarizer, and  $BS$  is a beam splitter. In the virtual mode, the target plane is located behind the SLM so the system size can be minimized.

#### A.1.4 Waveguide details.

Figure S4 shows the principle of the pupil replicating waveguide. See section 3.1.3 for more detailed information.

Figure S5 shows the experimental setup of the wearable display for the pupil-replicating waveguide test. The merged full-color collimated light was coming out through a hole on the wall, reflected by a folding mirror, coupled into the waveguide with a circle-shaped incoupler, and out-coupled over the outcoupler region as shown in the Fig. S6. The out-coupled light is collimated ( $\theta_c = 0$ ) as designed from the waveguide manufacturer. The out-coupled beam is not as uniform as the beam splitter-based benchtop prototype because of the mismatch between the designed incoherent light source and the implemented laser light source. The beam quality got worse when the beam didn't feed the entire in-coupler as shown in Fig. S6. However, the coherent length is preserved during the propagation and it is possible to form a holographic images with the SLM.

While the red and green laser diode in the system were well-matched to the designed wavelengths of the waveguide, the wavelength of the blue laser diode didn't match with the wavelength. As shown in Fig. S7, the efficiency of the blue was very low compared to the red and green. However, this is just a matter of waveguide design and the choice of the laser diodes. It is possible to make a waveguide specially designed for the Holographic Glasses.

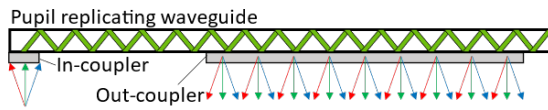


Fig. S4. Principle of pupil replicating waveguides which are usually used as image combiners in AR displays. The input light beam is in-coupled, totally internally reflected inside the waveguide, and out-coupled at the lossy grating. The input  $k$ -vectors are replicated over the out-coupler region.

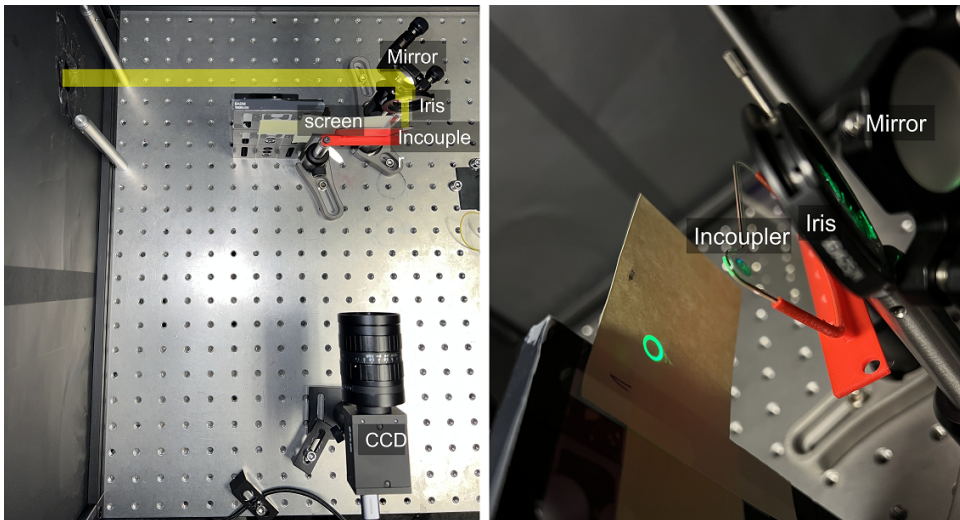


Fig. S5. Experimental setup for the pupil-replicating waveguide test. (left) The merged full-color collimated light was coming out through a hole on the wall, reflected by a mirror, shaped with an iris, and then met the in-coupler. (right) The circular shadow shows that the light rays are in-coupled.

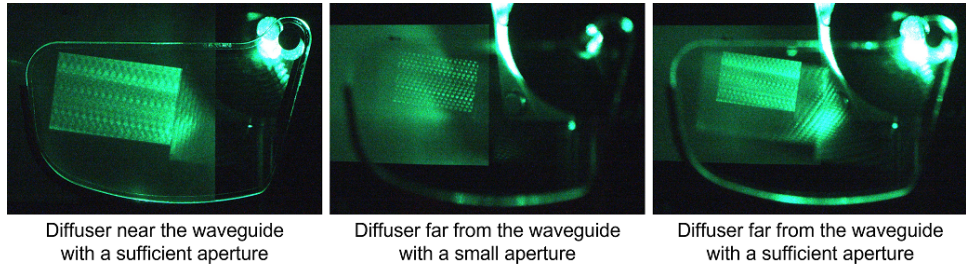


Fig. S6. Experimental result for the out-coupled illumination test. As shown in the left of Fig. S5, the diffuser was located (left) near distance with a sufficient aperture, (center) far distance with a smaller aperture, and (right) far distance with a sufficient aperture. Note that the out-coupled light was collimated and the illumination size didn't change over  $z$ -axis.

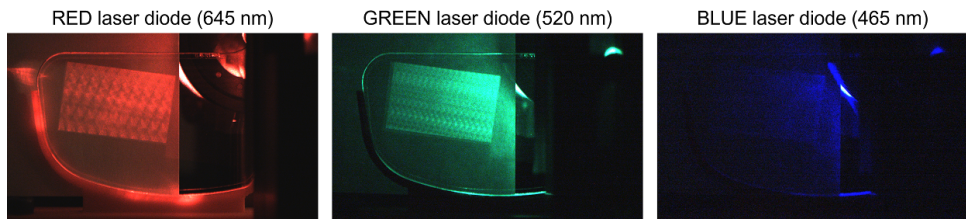


Fig. S7. Experimental result for the RGB illumination test. While (left) red and (center) green laser diodes' wavelengths were matched to the originally designed wavelengths of the waveguide, (right) the blue laser diode's wavelength didn't match with the waveguide's wavelength

## B ADDITIONAL CAPTURED RESULTS

Figure S8 shows the captured benchtop 2D results. The image quality and the color representation was very good considering the small form factor of the benchtop prototype. The red arrow shows the artifact because of the stray light from the SLM due to the GP lens loss. The HOGD-CITL algorithm presented better image quality and higher contrast, as expected. The 2D results from the wearable prototype showed worse image quality and contrast, as shown in Fig. S9. It is mainly because of the mismatch between the waveguide and the implemented coherent light source, which could be improved with a different grating design.

## C ADDITIONAL SIMULATED RESULTS

### C.1 Algorithm comparison

Figures S10 and S11 shows the simulated comparison for different algorithms with 6.4  $\mu\text{m}$  and 3.2  $\mu\text{m}$  SLM pixel pitch, respectively, when pupil diameter changes. The numbers inside the image indicate the PSNR value. As shown in Fig. 7 in the main manuscript, the pupil-HOGD shows the best results, especially when the pupil diameter  $w_t$  is smaller than the HDO interval  $w_h$ . HOGD works similarly good when the pupil diameter  $w_t$  is larger than the HDO interval  $w_h$ , because it assumes the HDOs are not filtered out and delivered to the user. However, DPAC shows surprisingly good results when the pupil is small, because the small pupil work as a Fourier filter that enables the DPAC mechanism (heavy filtering at the Fourier plane). However, it rapidly degrades as the pupil size gets bigger. With a smaller pixel pitch (3.2  $\mu\text{m}$ ), overall image quality goes up while the Pupil-HOGD shows the best image quality too.

### C.2 Robustness test

Since the pupil-HOGD requires precise measurement or control of the pupil diameter, it is worth to check the robustness of the pupil-HOGD algorithm: How does it work with a wrong pupil diameter parameter? As shown in Fig. S12, the Pupil-HOGD always shows better performance than the HOGD when the pupil diameter error is smaller than 0.5 mm. Note that the HOGD graph is almost identical to the black line (8 mm pupil-HOGD). So if we can measure or control the pupil with less than 0.5 mm error, Pupil-HOGD can always provide better image quality than the naive HOGD algorithm.

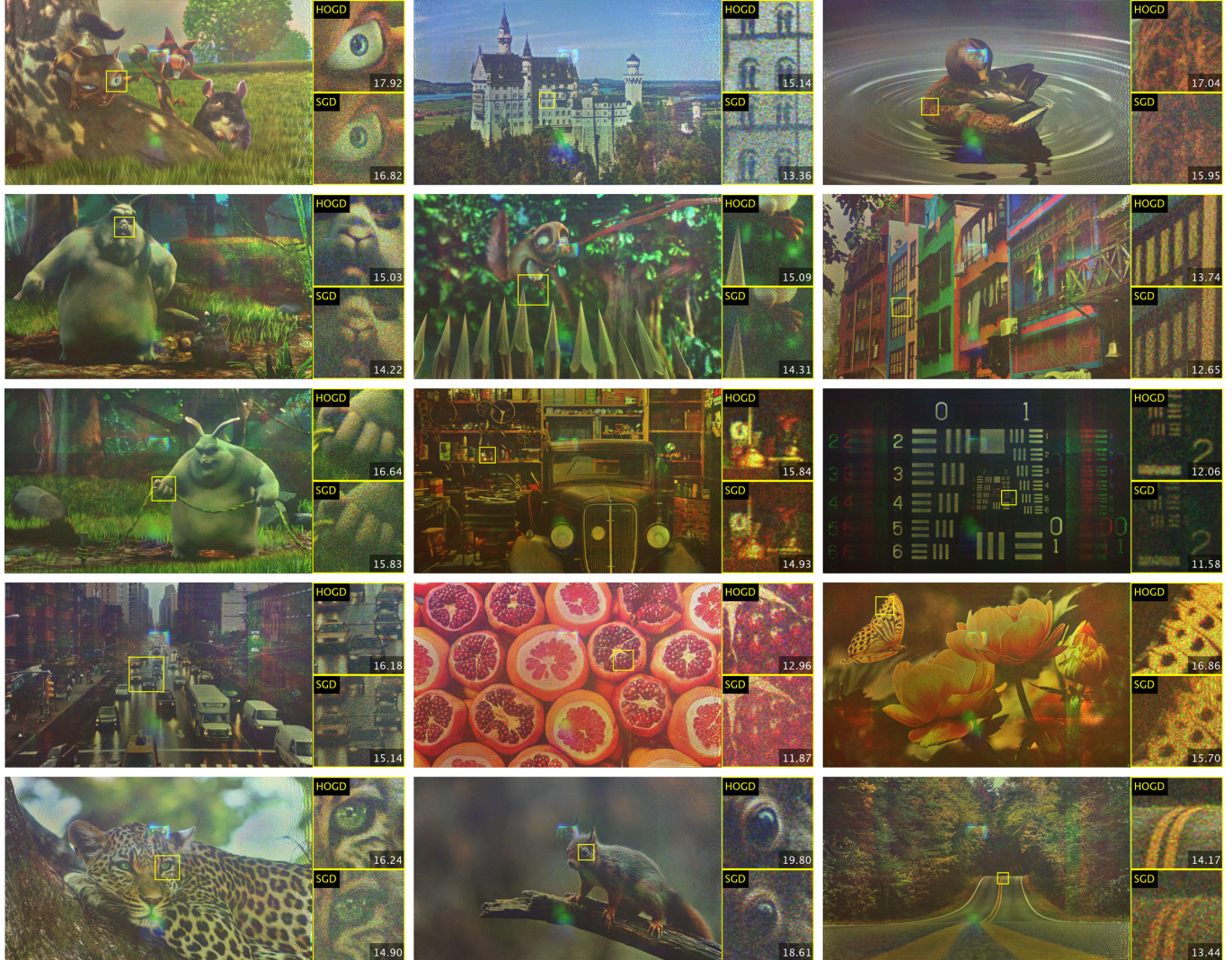


Fig. S8. Additional captured 2D results from the benchtop prototype.

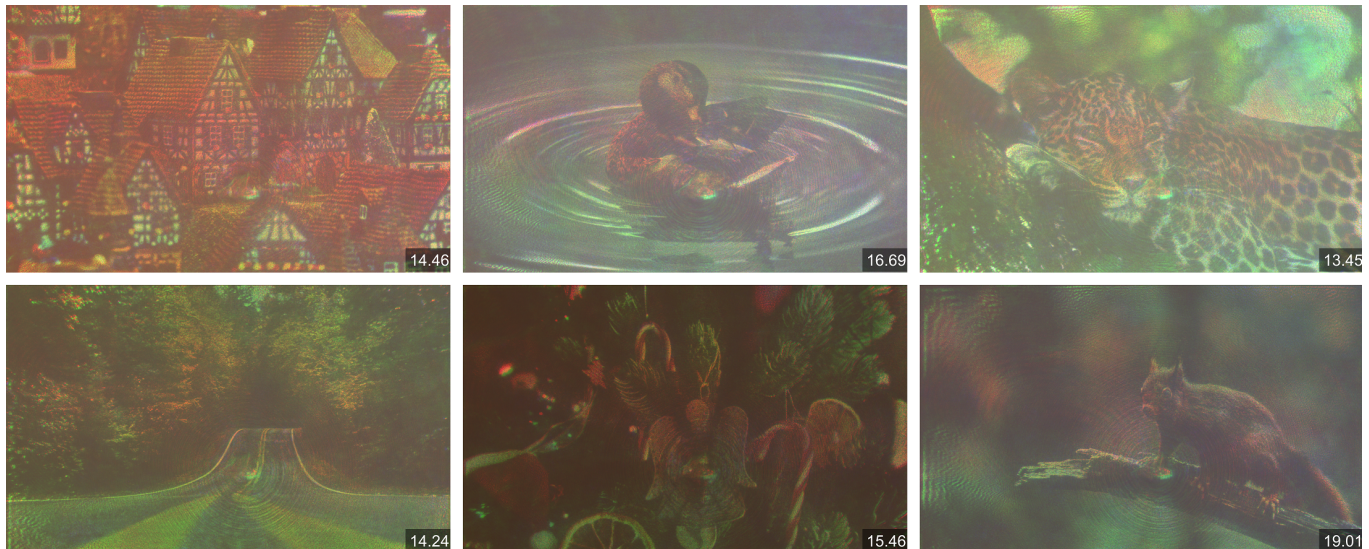


Fig. S9. Additional captured 2D results from the wearable prototype.

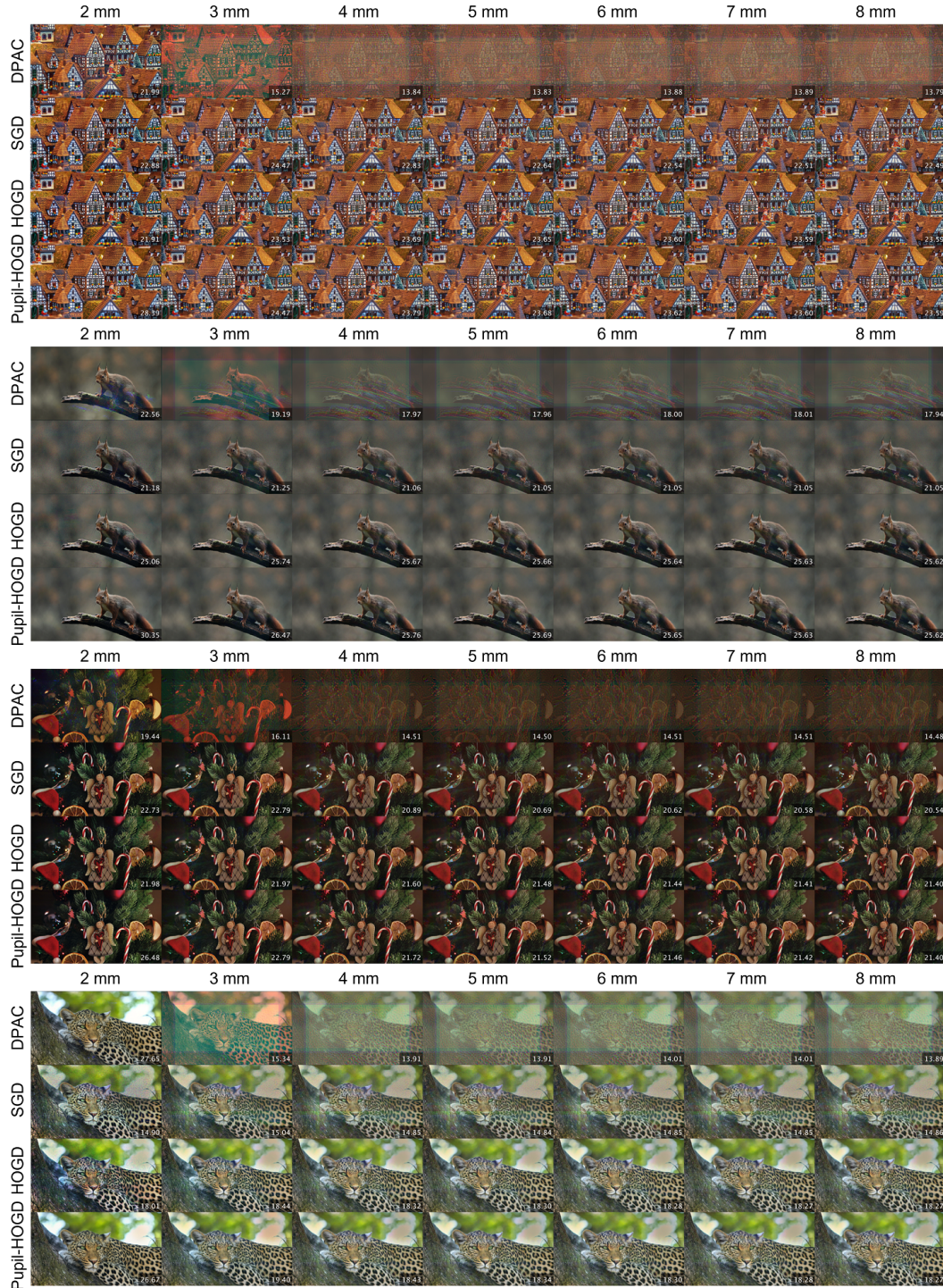


Fig. S10. Simulated comparison for different algorithms with 6.4um SLM pixel pitch, when pupil diameter changes.

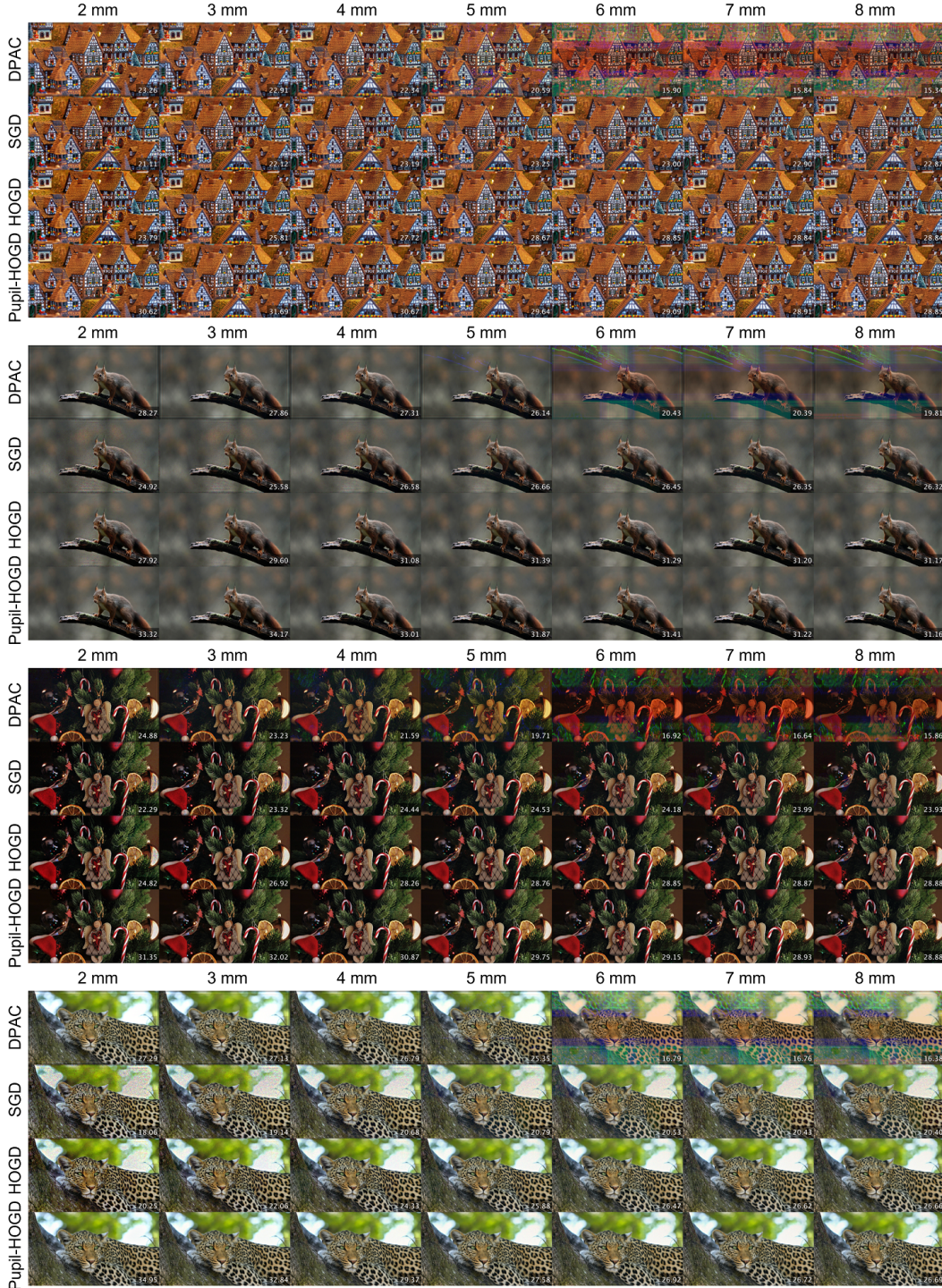


Fig. S11. Simulated comparison for different algorithms with 3.2um SLM pixel pitch when pupil diameter changes.

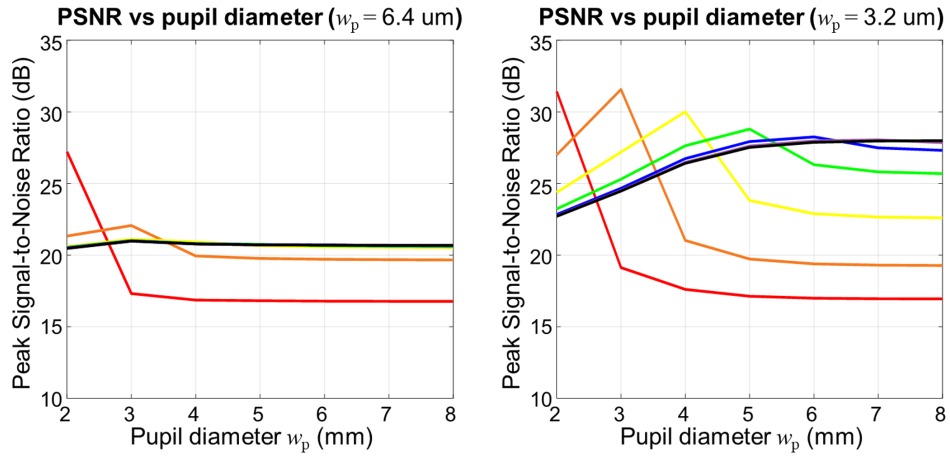


Fig. S12. The robustness test for the Pupil-HOGD. Each line shows the simulated PSNR results of the different pupil-HOGD algorithm when user's pupil diameter changes. red, orange, yellow, green, blue, dark blue, purple, and black line indicate the pupil mask size 2, 3, 4, 5, 6, 7, and 8 mm, respectively. Note that each algorithm has a maximum value when the pupil diameter matched to the pupil mask size. (left) robustness test with 6.4 um SLM pixel pitch (right) robustness test with 3.2 um SLM pixel pitch